EARTHQUAKE ENGINEERING AND STRUCTURAL DYNAMICS, VOL. 25, 435–463 (1996)

EFFECT OF MODELLING ASSUMPTIONS AND INPUT MOTION CHARACTERISTICS ON SEISMIC DESIGN PARAMETERS OF RC BRIDGE PIERS

A. S. ELNASHAI* AND D. C. McCLURE†

Department of Civil Engineering, Imperial College of Science, Technology and Medicine, London SW7 2BU, U.K.

SUMMARY

Modelling assumptions, boundary and loading conditions have a significant effect on analytical assessment of ductility supply and demand measures for RC bridges, a structural form which had suffered extensively in recent earthquakes. In recognition of the important role played by analysis in advancing seismic design of bridges, this paper is concerned with assessing the effect of model characteristics and earthquake strong-motion selection on analytical action and deformation seismic design parameters. This is of particular significance when viewed in the light of the large capital investment and problems with the satisfaction of dynamic similitude encountered in physical testing of piers and pier-deck assemblies. The models studied range between simple fixed-base cantilever and inclusion of both soil and deck effects, represented by assemblies of springs in translational and rotational degrees of freedom. Moreover, two sets of earthquake records are used in dynamic analysis, each comprising six records covering low, intermediate and high a/v, where a and v are the peak ground acceleration and velocity, respectively. The two sets differ in the scaling procedure employed to bring them to a common level of severity; the first set is obtained by direct acceleration scaling whilst the second utilizes the concept of velocity spectral intensity. The results from static and dynamic analysis, using advanced material characterization and solution procedures, are assessed and discussed. Subject to the limitations of the study, outlined in the paper, the results indicate that the inclusion of deck stiffness and/or soil representation is essential to avail of accurate seismic response parameters. However, the effect of variations in soil stiffness and/or deck torsional rigidity applied in the analysis is rather small, compared to the inclusion/exclusion of the model feature. Moreover, it is also observed that using acceleration scaling leads to much larger scatter in the results than when velocity spectral intensity scaling is used. Finally, the results from two particular earthquakes, Friuli and El Centro, highlight the peril of using a small number of records selected without due consideration to the relationship between their wave form, predominant periods and spectral shapes on the one hand and the response periods of the structure on the other.

KEY WORDS: seismic design; bridges; reinforced concrete piers; ductility; strong-motion scaling

1. INTRODUCTION

Seismic performance of reinforced concrete bridges has been attracting considerable attention, following the collapse of several structures in the San Fernando (1969), the Loma Prieta (1989) and the Northridge (1994) earthquakes in California. Concerns have been expressed regarding the safety of such structures in other parts of the world, in view of the belief that seismic design of bridges in California is quite advanced. This was further emphasized by the devastation of the transportation network due to the Hyogo-ken Nanbu (Kobe, Japan) earthquake of 17 January 1995. Notwithstanding the direct human and economic losses from the

* Professor of Earthquake Engineering
† Post-graduate student

CCC 0098–8847/96/050435–29

Received 15 August 1995
Revised 12 December 1995

heavy damage or collapse of a major bridge structure, the loss of an important transportation artery causes great damage to business, especially in affluent societies. This, reinforced by the field observations which indicate that there is a lot still to be learnt in seismic design of RC bridges, lends weight to the concerted effort dedicated to studying the inelastic seismic response of such structures, not only in California, but worldwide. Moreover, the imminent introduction of the Eurocode 8 chapter on Bridges has stimulated interest in this subject in Europe.

To evaluate the supply of RC bridges, required to meet the demand imposed by strong ground motion, experimental testing of components is required. Since small scale testing, particularly under dynamic loading, encounters problems of similitude, full, or near-full scale testing is preferable, rendering investigations of seismic supply of bridge components prohibitively costly. Therefore, analytical procedures, using material and member models which incorporate the salient behavioral representations, are of great significance. Analytical results may be verified by experimentation in a targeted and an optimally steered fashion. Issues of demand are not discussed herein, but it suffices to state that the case for utilization of analytical methods in demand assessment is even stronger than in supply estimation.

Having highlighted the role played by, and the potential of, analytical investigations of seismic supply of bridges, it is important to discuss the current capabilities for such procedures. Constitutive relationships for the two constituent materials, steel and concrete, have advanced considerably in recent years, with cyclic degrading models and passive instantaneously varying confinement for concrete, and with multi-surface plasticity formulations and mixed hardening rules for steel. Moreover, local reinforcement buckling and geometric second-order effects can be adequately accounted for. In spite of this, analytical results for similar structures vary enormously if undertaken by different research groups using different programs. A recent example is the study of a ten-span curved RC bridge used as a bench-mark for the 'Second International Workshop on Seismic Design of Bridges' held in New Zealand in August 1994. The results of earthquake analysis of the bridge presented by Petrangeli and Pinto,[1] Monti and Nuti,[2] Kodera *et al.*,[3] Kowalsky and Priestley,[4] Singh and Fenves[5] and Dodd *et al.*[6] vary enormously. This variation is attributed to modelling differences rather than to variations in the constitutive relationships used or the solution procedures adopted. This is confirmed by a recent comprehensive study of models used to represent the cyclic response of reinforced concrete structures undertaken by Chan and Mander.[7] Whereas differences exist, they are by no means spectacular, and would not account for the differences observed in the above-mentioned studies of the curved bridge.

To investigate the effect of modelling assumptions, and to provide general guidelines for the accurate modelling of RC bridges, this study focuses attention on a single pier–foundation–deck system. Various levels of modelling rigour are used and a selected set of seismic response parameters monitored. In addition to structural model details, aspects of input motion variation are briefly examined, in terms of the selection criteria of a suite of earthquake records, and the method of scaling acceleration time-histories.

2. ANALYTICAL MODELLING

To investigate the response of the bridge pier using different modelling assumptions, an accurate determination of inelastic deformations in reinforced concrete is necessary. Such analysis requires material constitutive models and accurate member representation to predict the behaviour. In this section a brief account of the numerical element types and constitutive material models is given.

2.1. Element formulation and material models

To determine accurately member response, the advanced analysis program ADAPTIC (developed and verified at Imperial College) was used, employing fibre elements with transformations from elemental chord to global axes to account for large displacements. The fibre element formulation adopts a cubic shape function and permits the spread of inelasticity across its cross section and along its length. Inelastic behaviour is defined in terms of the selected constitutive material laws, with a check on the stress state carried out at a series of monitoring points. The reinforcement steel material model used was the commonly cited

bilinear kinematic hardening stress strain relationship, while a uniaxial cyclic model (Reference 8) was applied, including the significant effects that determine concrete behaviour, such as passive confinement and cyclic degradation.

Modelling of the soil stiffness and deck stiffness was performed using joint element springs with decoupled shear, axial and moment behaviour.

2.2. *Estimation of concrete confinement factors*

Confinement has a major influence on the response of concrete in its principal direction and thus is a significant parameter in the concrete constitutive model. Two simplified procedures were considered for the calculation of confinement factors: first the approach set out in Eurocode 8;[9] and the second another empirical relationship derived by Mander *et al.*[10]

According to the EC8 approach, the confinement factor K_σ is given by

$$K_\sigma = \begin{cases} 1{\cdot}0 + 5{\cdot}0\alpha_c \dfrac{f_l}{f_{co}} & \text{for } \dfrac{f_l}{f_{co}} < 0{\cdot}05 \\ 1{\cdot}125 + 2{\cdot}5\alpha_c \dfrac{f_l}{f_{co}} & \text{for } \dfrac{f_l}{f_{co}} \geqslant 0{\cdot}05 \end{cases} \tag{1}$$

The equation given by Mander *et al.*[10] is as follows:

$$K_\sigma = -1{\cdot}125 + 2{\cdot}254\sqrt{1 + 7{\cdot}94\alpha_c \frac{f_l}{f_{co}}} - 2\alpha_c \frac{f_l}{f_{co}} \tag{2}$$

where

$f_l = \dfrac{\rho_s f_{sy}}{2}\left(1 - \sqrt{\dfrac{S_{sp}}{1{\cdot}25d_{cc}}}\right)$

f_{co} is the compressive strength of unconfined concrete,
f_l is the confining pressure,
α_c is the confinement effective coefficient,
ρ_s is the volumetric ratio of confining steel,
f_{sy} is the yield strength of confining stirrups,
S_{sp} is the spacing of the confining stirrups and
d_{cc} is the diameter of the confined concrete core.

Whereas both expressions are based on the assumption of the simultaneous attainment of yield in steel and peak stress in concrete, the use of more rational passive confinement models was not considered necessary, since this study is aimed at establishing comparative measures of response assessment under different modelling assumptions. Moreover, there is no clear technical argument in favour of either of the above expressions; hence the more conservative EC8 approach was adopted.

3. RESPONSE CRITERIA AND LIMIT STATES

In order to determine seismic response parameters in both the static and dynamic analyses, it is necessary to define a set of limit states for yield and ultimate. The limit state definition remains controversial and results obtained from one study are not, in general, comparable to another due to the wide variation in this definition. These are discussed hereafter, in the light of the wider discussion presented by Elnashai and Beith.[11]

3.1. *Yield limit state*

The criteria initially considered for yield were two established definitions: first yield of the longitudinal reinforcement; and the secant of the load deflection curve.

(i) *First yield.* First yield is defined as the point at which the main longitudinal reinforcement reaches the material yield strain. Problems exist with this definition in terms of numerical estimates when compared to experimentally obtained values. Generally, values observed experimentally tend to be greater than those obtained numerically. This arises from bond slip between the longitudinal reinforcement and the concrete, combined with early stiffness degradation due to cracking of the section. It was decided that the point of first yield would not in fact be taken when the outer-most pair of reinforcement bars yielded, as this was seen to have minor overall effect. Instead, the point of first yield was taken to coincide with yielding of five reinforcement bar pairs. This was verified by mapping the load–displacement curve onto the stress–strain curve of the reinforcing bars. A departure from linearity was observed closer to the yielding of five bars than otherwise. This is clearly a function of the particular structure considered and may require re-assessment for a different configuration.

(ii) *Secant yield.* A commonly employed definition of yield is used herein whereby the yield displacement of the system is equal to that of an equivalent linearly elastic-perfectly plastic system. The latter has an initial stiffness given by the point of intersection of the line at 75 per cent of ultimate load with the load–displacement curve of the inelastic system. The plastic load of the equivalent system is taken as the ultimate load of the inelastic system.

3.2. Ultimate limit state

Even more than the yield limit state, the definition of ultimate structural response is a particularly subjective decision. Consequently a number of ultimate criteria were considered, as follows:

(i) *Concrete failure.* This definition is based on an approach used by Lappas and Tassios,[12] who defined the point of ultimate limit state from the maximum available curvature. This curvature is assumed to correspond to the post-peak value of curvature at 0·85 of the peak moment, M_{peak}. Multiplying this value of curvature by a fictitious, but conservative, value of plastic hinge length $L/4$, the corresponding maximum available rotation is obtained. In the case of the pier under investigation the axial load remains unaltered. This implies that the curvature at failure would be constant and thus the value of strain at 0·85 M_{peak} would also correspond to failure. Finally, the stress in the confined concrete is related to the moment, therefore the ultimate strain could alternatively be calculated from a 15 per cent drop in the peak stress of the confined concrete.

(ii) *Significant drop in resistance.* A commonly cited criterion that is based on prescribing the ultimate limit state as the deformation corresponding to a drop in the load carrying capacity of the load–deflection curve, typically in the range of 5–10 per cent.

(iii) *Fracture of tensile reinforcement.* This criterion defines the ultimate limit state using a limiting value of tensile strain in the main longitudinal reinforcement. The limiting value of strain is taken as that permitted in Eurocode 8, which is 12 per cent.

(iv) *Limit on excessive rotation.* An empirical procedure essentially limiting element rotation may be utilized. Using such a definition of ultimate limit state constrains the rotational ductility to a predetermined value.

4. LIMIT STATES AND RESPONSE PARAMETERS

To assess the results generated in both the monotonic and dynamic analyses a series of response parameters must be defined. Parameters of most interest in seismic design are deflection, rotation and curvature ductilities as well as plastic hinge length. These parameters collectively reflect the capacity of the structure of absorb and dissipate the input earthquake energy.

4.1. Yield criteria

As discussed in Section 3.1, two yield criteria were considered, namely, first yield and secant yield. Initial tests showed that both criteria were in close agreement for the case of fixed base models. As greater degrees of flexibility at the pier support were introduced through modelling assumptions, a disparity became evident.

This could be attributed to greater involvement of P–Δ moments resulting from rigid body rotations at the pile cap. In such cases the load–deflection curves peak at lower values and at larger displacements. This in turn gave significantly larger values of yield displacement based on secant yield. These yield values were not considered representative after inspection of the level of strain imposed on the main reinforcement. To avoid such disagreement the yield criterion became solely defined using first yield.

4.2. Ultimate criteria

With regard to ultimate limit state mentioned in Section 3.1 fracture of the main reinforcement at the ultimate material strain of 12 per cent was never achieved in initial tests. Therefore, three criteria were utilized, namely limiting strain level of confined concrete, excessive rotation limit and significant drop in resistance.

4.3. Response parameter calculations

The adoption of one yield and three ultimate limit state definitions furnished three values of each response parameter, for each modelling assumption. This in effect gave each parameter a band of values with an upper and a lower bound.

(i) *Class 1 response parameters.* This set of parameters were evaluated using first yield associated with the ultimate limit state defined in terms of the limit on excessive member rotation. Definition of ultimate conditions in such a manner constrains the rotational ductility. This consequently necessitates a predetermined knowledge of the likely response for such a structure and structural material. A value of $\mu_\theta = 8$ was assumed from previous work carried out by Elnashai and Beith,[11] and was subsequently found to give rather more conservative estimates of ultimate values. Class 1 can be considered as the lower bound set of parameters.

(ii) *Class 2 response parameters.* This class utilizes the strain corresponding to a 15 per cent drop in peak stress of the confined concrete stress–strain relationship as the ultimate condition.

(iii) *Class 3 response parameters.* The final set of parameters are calculated using the significant drop in resistance definition. A drop of 5 per cent in the load deflection response curve was chosen. This produced the largest estimates of ultimate limit state response parameters and thus this final class represents the upper bound.

5. STRUCTURAL MODELLING ASSUMPTIONS

The initial study of modelling assumptions was aimed at assessing the effect of varying the degree of structural complexity. Each modelling assumption adopted is discussed in the following sections in terms of physical nature and the subsequent numerical format. The structural models considered represent the progressive steps in modelling complexity that might be undertaken in a design office environment.

The fundamental pier model chosen for the study was obtained from an international collaborative study of a 3-D RC curved bridge which was presented in a workshop held in New Zealand.[13] Whereas the workshop was concerned with the global response of bridges as a whole, the purpose of the current study was to investigate the modelling and response of piers. Thus, a typical pier design was selected from the brief given in Reference 13, as shown in Figure 1.

The generic pier had the following parameters:

Cylinder compressive strength f_{cu}	35 MPa
Concrete tensile strength f_t	3 MPa
Characteristic steel yield f_y	430 MPa
Ultimate strength (at 12 per cent strain) f_u	665 MPa
Strain at yield ε_y	$2{\cdot}15 \times 10^{-3}$
Strain hardening parameter	1·0 per cent
Pier diameter	1500 mm
Pier height	7500 mm

Main longitudinal reinforcement	48D32 in pairs over the full height
Transverse reinforcement	D12 @ 70 mm centres for the bottom 20 per cent of the pier
	D12 @ 140 mm centres for the remainder of the height
Confinement factor K_a	1·026 for the bottom 20 per cent of the pier
	1·010 for the remainder of the height

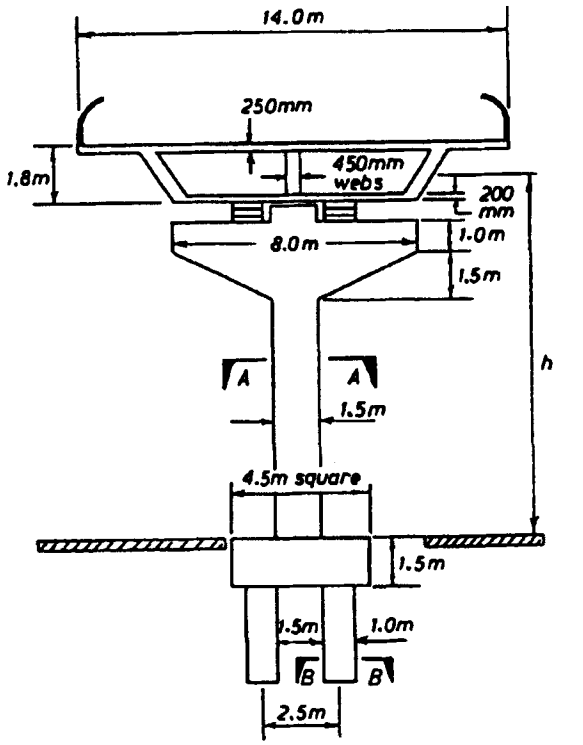

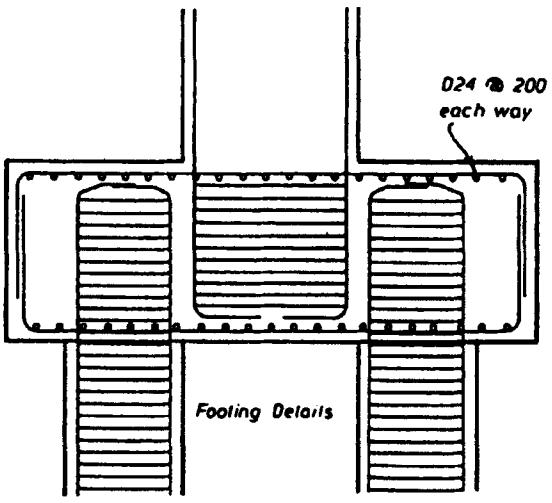

Figure 1(a). Pier and footing details.

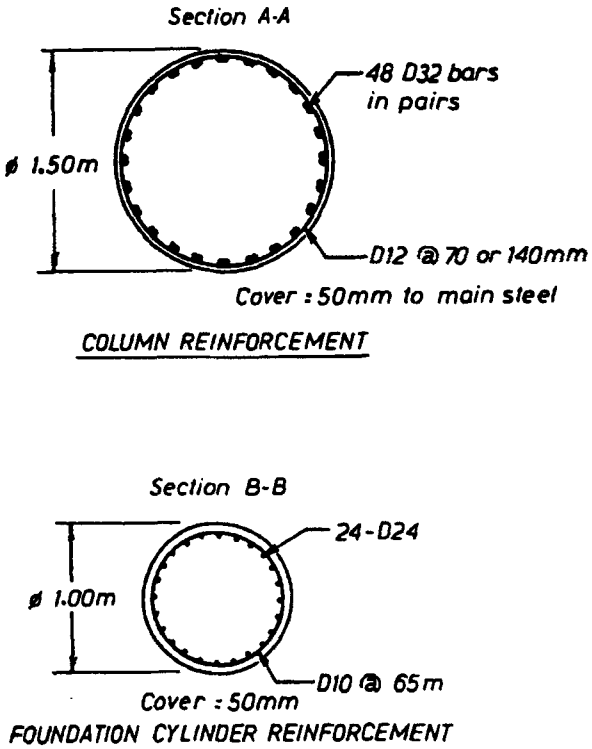

Figure 1(b). Pier column and pile reinforcement details

The section shear capacity is given by the summation of contributions from the concrete V_c, steel reinforcement V_s and axial force V_p.

$$V_{tot} = V_c + V_s + V_p \tag{3}$$

where

$$V_c = 0{\cdot}8 A_{gross} k \sqrt{f'_c} \tag{4}$$

$$V_s = \frac{\pi}{2} A_{sp} \frac{f_{ys} D'}{s} \cot 30 \tag{5}$$

$$V_p = PD/L \tag{6}$$

In these equations, A_{gross} is the cross-sectional area of the concrete, k reflects the degradation of shear strength with increasing displacement ductility, D and D' are the diameters of the pier and the confined concrete core, L is the height of the pier and P is the axial load acting on the pier. Subject to axial force and moments, the following equations describe the variation of k with pier displacement ductility, μ_Δ:

$$0 \leqslant \mu_\Delta \leqslant 1: \quad k = 0{\cdot}29 \tag{7a}$$

$$1 \leqslant \mu_\Delta \leqslant 3: \quad k = 0{\cdot}29 - 0{\cdot}095(\mu_\Delta - 1) \tag{7b}$$

$$3 \leqslant \mu_\Delta: \quad k = 0{\cdot}10 \tag{7c}$$

Application of the relevant material properties and dimensions to equations (3)–(6) gave a shear capacity $V_{tot} = 4855$ kN.

Finally, due to symmetry of the section, two-dimensional analysis is deemed sufficient for the purpose of the study. Furthermore the response of multi-span bridges in the longitudinal direction has been shown to be less significant, compared to the response in the transverse direction, Monti and Nuti.[2]

5.1. Pier model as a simple cantilever (MS1)

A control model was chosen as the simplest form that would be selected in a design office to carry out preliminary calculations. A fixed base pier acting as a simple cantilever was therefore considered, denoted by MS1.

Numerical modelling of the tapered section was implemented by splitting the taper into three 0·5 m subsections, and applying the mid-height properties of each subsection to the respective element. Due to its high flexural stiffness the taper section was unlikely to exhibit appreciable deformations. The pier column was discretised using five elasto-plastic elements each of 1·0 m length. Finally the base node was fixed in translation x, y and rotation about the z axis, thus forming a perfectly idealized cantilever, as shown in Figure 2. Since the tapered section was explicitly modelled, the deck weight was added at its natural location, with no recourse to the use of rigid links.

The majority of axial load developed in the pier evolves from the 40 m length of deck it supports. Consequently a concentrated load was imposed at the pier tip to represent the deck weight, in addition to distributed self-weights of particular importance for the rather heavy taper section.

5.2. Control model with plastic zone mesh refinement (MS2)

The first modelling assumption investigated was aimed at assessing how the level of discretization would affect the structural response. The cubic elasto-plastic element employed in the pier mesh displays a high degree of versatility in its ability to permit the spread of plasticity. However, it was deemed that if a coarse mesh was used, the location of the Gauss point closest to the base may not permit an accurate assessment of the behaviour of the most critical section in the pier.

The pier mesh was subsequently reconstructed with a degree of refinement such that base elements were limited to 500 mm or approximately $L/10$. This modelling assumption would thus provide a yard stick to the maximum distance from the base to the first integration station needed for accurate prediction of local and global structural response.

5.3. Pier models incorporating foundations (MS3 and MS4)

The first stage of additional model complexity that might be envisaged in analysis would be to include the influence of foundation effects. A two-stage approach was considered. Firstly to model the pile and pile cap

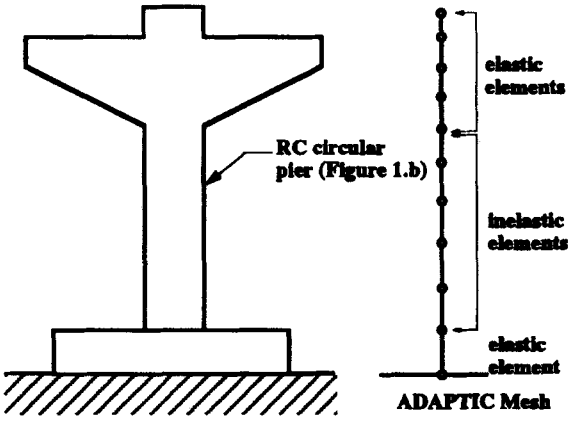

Figure 2. Modelling assumption MS (1) (control model)

but to neglect the soil and secondly to include the soil properties. The former was included in this study as an additional case of the latter (soil stiffness sensitivity) when the soil stiffness approaches zero.

5.3.1. Pier model with foundation structure — no soil effects MS(3). Details of the pile group design were adopted from previous studies,[13] as shown in Figure 1. The piles are of drilled type and extend to a depth of 5 m in cohesionless sand, at which point they are assumed to end bear on bed rock. Pile group reinforcement is given below:

pile	
Main longitudinal reinforcement	24D24 over the full length
Transverse reinforcement	D10 spirls with 65 mm pitch for the full height
pile cap	
Main reinforcement	D24 @ 200 mm centres each way top and bottom
Transverse reinforcement	D16 @ 400 mm centres each way

On the assumption that the piles are end-bearing, pinned supports were used to represent the socketing connection made in rock. Although the provision of pinned supports would prevent vertical freedom at the pile base, a situation which would not be achieved in reality, preliminary tests showed that no uplift developed at the rock–pile interface. With the possibility that inelastic behaviour could ensue in the piles, elasto-plastic elements were utilized. Due to the size of the pile cap and level of reinforcement specified, it was deemed that only elastic deformations would prevail in this section. Thus to reduce any unnecessary computational effort, the pile cap was idealized using a solid steel cross section with a structural stiffness identical to that of the reinforced concrete pile cap. A diagrammatic representation is shown in Figure 3.

5.3.2. Pier model with foundation structure — including soil (MS4). Having considered the extreme case of including the influence of foundation structure but neglecting the soil, a further series of models were set up to assess the sensitivity of parameter response to soil stiffness. The value of lateral subgrade coefficient quoted in

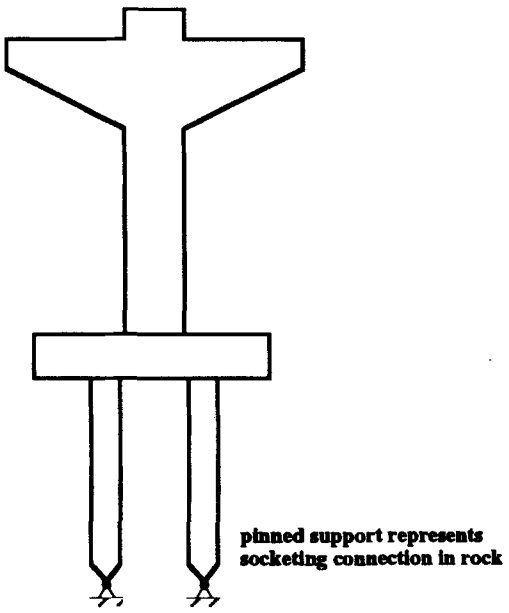

Figure 3. Modelling assumption MS (3) (pier incorporating foundation structures, nil soil stiffness)

Reference 13 was selected as a benchmark for typical soil stiffness of cohesionless sand. By multiplying and dividing this value using a factor of two, a range of values were generated to represent the limits of possible soil stiffness.

Whereas modelling the soil may be performed using continuum finite and boundary element procedures, within the context of structural analysis, spring representation is sufficient. This is the approach adopted here, after considering more complex mechanical analogue models available in the literature. For lateral loading the spring compliances are usually referred to as p–y curves. As a first approximation, the soil response was considered linear. To arrive at the value of soil spring stiffness the value of lateral subgrade coefficient given in Reference 13, which is a function of depth, was calculated as a piece-wise constant function of depth, with a step equal to the pile element mesh spacing. The total force resulting from the continuous soil reaction was modelled as a discrete spring force. The springs have equal tension and compression characteristics. Since the piles are end-bearing, no vertical springs were used for skin friction representation. Modelling of vertical stiffness of the soil located underneath the pile cap was neglected, on the premise that this material would be back fill of negligible strength. The model used in shown in Figure 4. In this analysis, the mass of the soil as well as its radiation damping characteristics were not included. This decision was taken since very few practical analyses of bridges go that far in complexity and the ensuing number of parameters (accounting for soil properties other than stiffness and strength) would have been prohibitively large. Finally, no group effects were taken into consideration, for the latter reasons.

The models set up to represent the range of soil stiffnesses were denoted as follows: MS4a low soil stiffness, MS4b medium soil stiffness and MS4c high soil stiffness.

5.4. Pier incorporating foundation and deck influence (MS6)

As a further level of model elaboration that might be contemplated in analysis, a provision was made for possible deck stiffness that could be mobilized due to the type of pier-deck support condition. Under pier loading transverse to the plane of the deck, support bearings could generate a certain degree of torsional moment. An upper bound value of available moment would exist when the entire deck load would be transferred to one bearing. Assuming a spacing of bearings from the pier centre line of 3·5 m, this would correspond to a moment of 19·4 M Nm, based on the dead and live loads on the deck acting equally at the

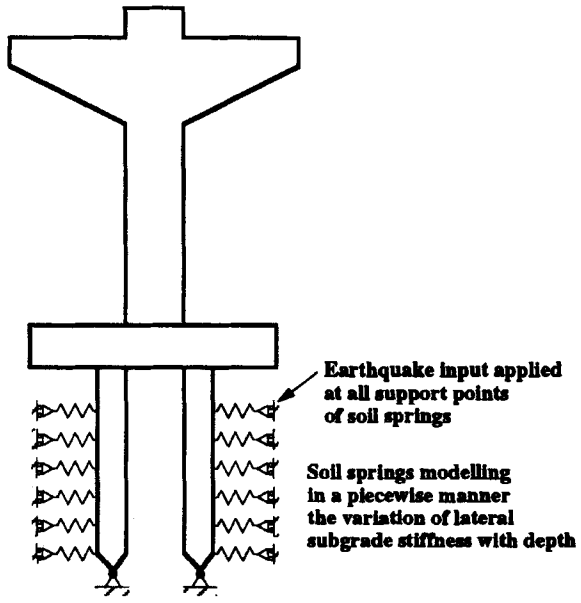

Figure 4. Modelling assumption MS (4) (pier incorporating foundation structure and soil stiffness)

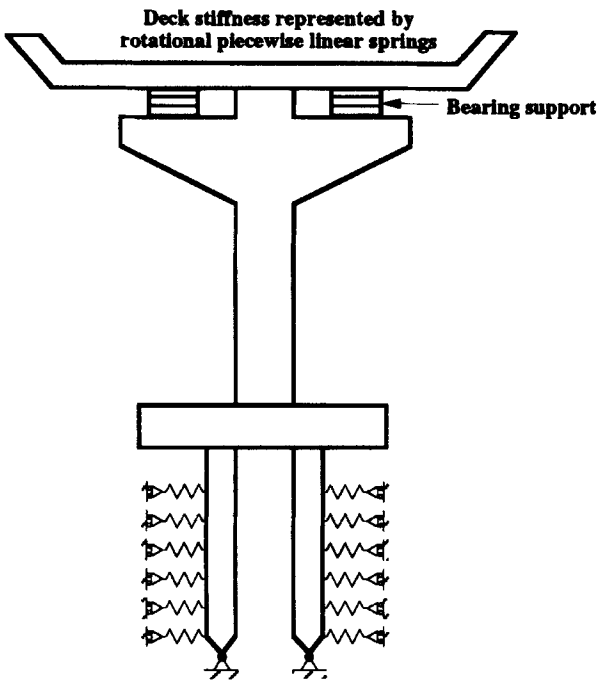

Figure 5. Modelling assumption MS (6) (pier incorporating foundation structure, soil stiffness and deck restraint)

two bearing support points. In the absence of any data with regard to the performance of bearings, it was assumed that they would possess adequate rigidity such that the full deck torsional stiffness would be developed. A joint element, similar to that used for soil property modelling, was employed with zero axial and shear component but with a rotational stiffness corresponding to that of the deck. Moment-rotation characteristics for the element were implemented using a bilinear curve with initial stiffness equal to the torsional stiffness of the deck up to the point of maximum available moment given above. Beyond this, zero stiffness gradient was defined to limit the maximum developed moment. Considering a typical pier from the literature (Reference 13), the torsional constant J was calculated as 11·7 m^4, whilst the torsional stiffness k_θ was $22{\cdot}44 \times 10^{12}$ Nm/rad. A graphical representation of the model is shown in Figure 5.

In a manner similar to soil stiffness, three models of deck stiffness were set up to assess the sensitivity of the response parameters to the deck torsional restraint. However, due to the nature of hollow sections where stiffness vary dramatically with minor changes in cross section dimensions, a factor of five was chosen for scaling the stiffness to both magnify and reduce the above value.

The mid-range value of lateral subgrade coefficient was used for the case of models incorporating deck stiffnesses and foundations. The models thus generated were denoted MS6a in the case of low deck stiffness, MS6b in the case of medium deck stiffness and MS6c in the case of high deck stiffness. Model MS5 includes deck restraint but no soil–foundation system (justified in Section 6.2).

6. RESULTS FOR MONOTONIC LOADING

Results discussed hereafter are divided into two categories, namely, models including deck torsional stiffness and free cantilevers, since the mode of response of the two systems is fundamentally different. Whereas models including deck stiffness behave as shear frames, those possessing no deck stiffness respond as simple cantilevers.

6.1. Models possessing no deck stiffness

6.1.1. Control model — simple cantilever pier (MS1). Results of the pier acting as a pure cantilever form the basis for comparison with the other model assumptions in this category. Moreover, with reference to Section 4.1.3, Class 1 response parameters represent the lower bound, Class 2 the mid-range and Class 3 the upper bound values. The results from the static analysis are summarized in Tables I–IV and presented in load deflection curves as shown in Figures 6–9.

Displacement ductility results display a range of values in which $4{\cdot}2 \leqslant \mu_\Delta \leqslant 6{\cdot}3$. Taking the lower bound value, this compares favourably with the conservative values quoted in codes of practice for reinforced concrete structures. Values calculated for rotation and curvature ductility also echo values obtained by Elnashai and Beith[11] in a similar investigation on ductility capacity of soild circular RC piers. Little variation occurs for values of plastic hinge length calculated using either class of ultimate criteria, and these too agree with values quoted by Elnashai and Beith.[11]

6.1.2. Control model with plastic zone mesh refinement (MS2). Initial observations of the refined mesh model result suggested little change in response with the load deflection curve of Figure 6 matching nearly

Table I. Displacements at yield and ultimate limit state. Structural state at yield and ultimate conditions

	Yield			Ultimate, Class 1			Ultimate, Class 2			Ultimate, Class 3		
Model	Δ (mm)	θ (rad $\times 10^{-3}$)	ϕ ($\times 10^{-3}$)	Δ (mm)	θ (rad $\times 10^{-2}$)	ϕ ($\times 10^{-2}$)	Δ (mm)	θ rad $\times 10^{-2}$)	ϕ ($\times 10^{-2}$)	Δ (mm)	θ (rad $\times 10^{-2}$)	ϕ ($\times 10^{-2}$)
MS1	49	2·760	2·884	205	2·208	2·350	220	2·440	2·590	310	3·687	3·990
MS2	47	1·396	2·852	150	1·112	2·360	160	1·266	2·557	370	3·840	8·860
MS3	102	2·754	2·875	310	2·200	2·400	318	2·430	2·601	400	3·600	3·880
MS4a	86	2·764	2·889	261	2·211	2·365	276	2·425	2·590	360	3·580	3·860
MS4b	77	2·742	2·871	247	2·194	2·356	263	2·425	2·594	340	3·650	3·900
MS4c	70	2·770	2·890	240	2·216	2·330	260	2·460	2·630	330	3·700	3·950
MS5	15	2·560	2·921	90	2·050	2·550	81	1·805	2·258	260	5·760	8·645
MS6a	146	2·572	2·927	365	2·050	2·540	358	1·836	2·285	580	6·918	11·096
MS6b	110	2·550	2·921	345	2·050	2·560	330	1·810	2·278	580	7·463	11·950
MS6c	100	2·552	2·890	340	2·040	2·500	325	1·845	2·237	570	7·220	11·690

Table II. Ductility parameters for classes 1–3. Response parameters

	μ_Δ			μ_θ			μ_ϕ		
Model	Class 1	Class 2	Class 3	Class 1	Class 2	Class 3	Class 1	Class 2	Class 3
MS1	4·2	4·5	6·3	8·0	8·8	13·4	8·1	9·0	13·8
MS2	3·2	3·4	7·9	8·0	9·0	27·5	8·3	9·0	31·1
MS3	3·0	3·1	3·9	8·0	8·8	13·1	8·2	9·0	13·5
MS4a	3·0	3·2	4·2	8·0	8·8	13·0	8·2	9·0	13·4
MS4b	3·2	3·4	4·4	8·0	8·8	13·3	8·2	9·0	13·6
MS4c	3·4	3·7	4·7	8·0	8·9	13·4	8·1	9·1	13·7
MS5	6·0	5·4	17·3	8·0	7·1	22·5	8·8	7·7	29·6
MS6a	2·5	2·5	4·0	8·0	7·1	26·9	8·7	7·8	37·9
MS6b	3·1	3·0	5·3	8·0	7·1	28·4	8·8	7·8	40·6
MS6c	3·4	3·3	5·7	8·0	7·2	28·3	8·8	7·7	41·0

Table III. Yield and ultimate loads. Yield and collapse loading

Model	Yield force (kN)	Collapse force (kN)			Yield moment (kN m)	Collapse moment (kN m)		
		Class 1	Class 2	Class 3		Class 1	Class 2	Class 3
MS1	1483	1862	1853	1792	11 460	15 400	15 420	15 500
MS2	1450	1872	1870	1781	11 500	14 900	14 970	15 600
MS3	1468	1834	1830	1790	11 440	15 400	15 400	15 600
MS4a	1474	1845	1840	1780	11 400	15 400	15 400	15 600
MS4b	1470	1839	1850	1787	11 500	15 400	15 400	15 600
MS4c	1475	1849	1850	1782	11 500	15 400	15 400	15 600
MS5	4740	6850	6840	6510	11 500	17 500	17 400	17 290
MS6a	4650	6727	6713	6411	12 400	17 400	17 400	17 230
MS6b	4220	6691	6650	6384	12 300	17 400	17 300	17 200
MS6c	4068	6698	6647	6381	12 130	17 400	17 350	17 200

Table IV. Plastic hinge lengths and energy absorbed. Plastic hinge lengths

Model	Normalized hinge length			Absorbed hinge energy (kN m)
	Class 1	Class 2	Class 3	
MS1	0·257	0·256	0·261	317 103
MS2	0·232	0·228	0·263	165 881
MS3	0·257	0·257	0·262	316 562
MS4a	0·255	0·255	0·265	315 252
MS4b	0·260	0·260	0·269	315 812
MS4c	0·253	0·253	0·263	315 920
MS5	0·282	0·286	0·289	227 203
MS6a	0·287	0·287	0·291	227 193
MS6b	0·289	0·293	0·295	227 753
MS6c	0·281	0·285	0·288	228 644

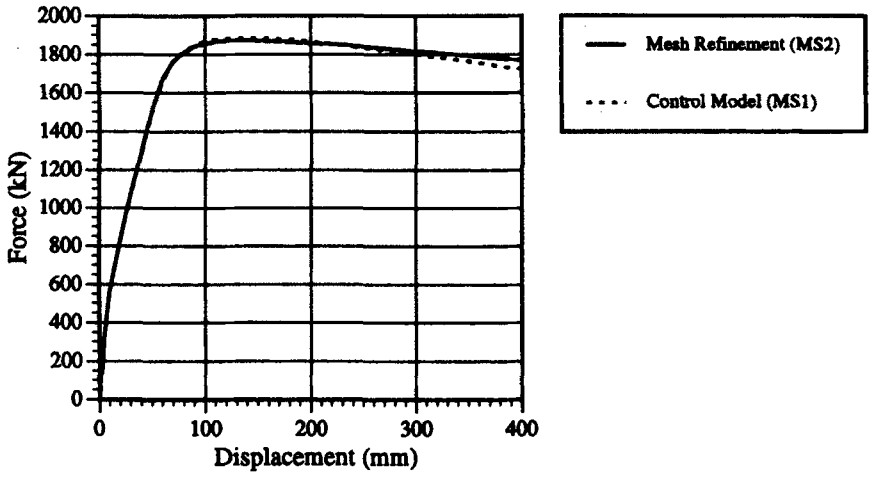

Figure 6. Load deflection curve for control and mesh refined models

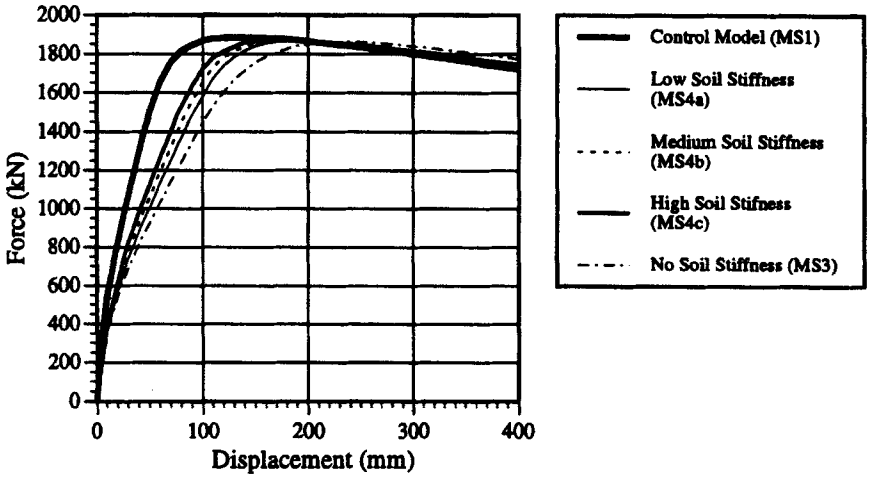

Figure 7. Load deflection curve for control model and models possessing foundation structure

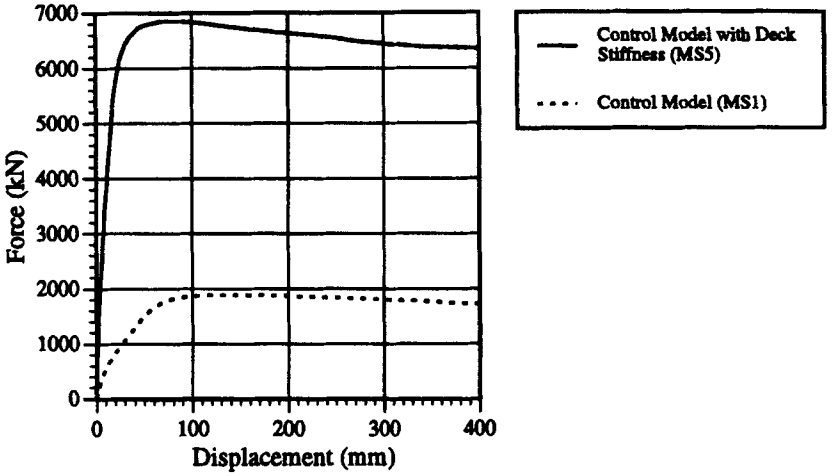

Figure 8. Load deflection curve for control model with and without deck stiffness

exactly the curve obtained for the control model. However, on calculation of the response parameters some variations did emerge. Class 1 and 2 displayed values of rotational and curvature ductility consistent with those of the control. This should be expected as the failure criteria for both these classes are based on rotation and strain. In the absence of any change in axial load these parameters should remain the same. Displacement ductility values, on the other hand, suffered a 25 per cent drop. This reduction obtained for μ_Δ can be seen to result from more accurate modelling of inelasticity at the critical section, in turn causing earlier achievement of failure criteria. Referring to Table I values of displacement at yield are in close agreement, taking the mid-range values of 49 mm for the control model and 47 mm for the refined mesh model. In contrast, the levels of displacement at ultimate display large variation being 220 mm for the control model as compared to 160 mm for the refined mesh model. Furthermore, as the plastic hinge length is a function of both μ_Δ and μ_ϕ, a commensurate reduction is observed in the plastic hinge length.

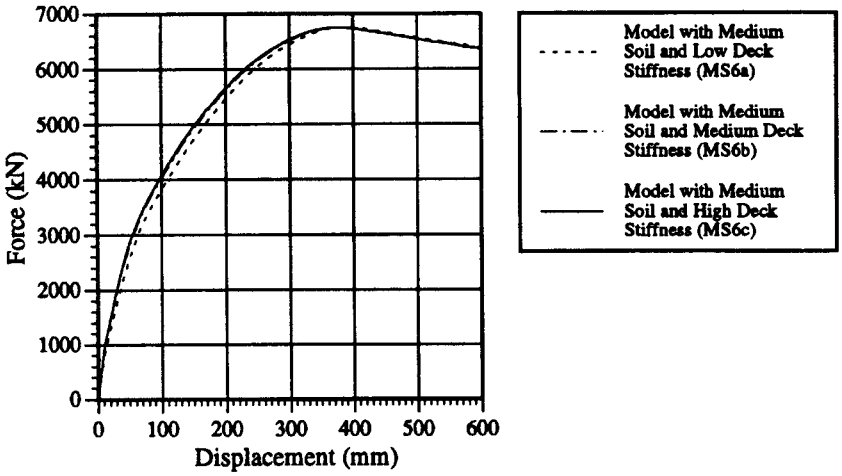

Figure 9. Load deflection curve for control model with deck stiffness and pier incorporating foundation and deck influence

With regard to the Class 3 response parameters, a significant increase of all three ductilities occurred. A 25 per cent increase was recorded for μ_Δ while values of μ_θ and μ_ϕ doubled. Such levels of increase can take place for sectional parameters and yet only cause minor variations in the overall μ_Δ because of the short length of element over which they take place. All of these increases nonetheless can be attributed to the milder dip which occurs beyond the peak lateral force in the load deflection curve. Since Class 3 is based on a significant drop in resistance, the displacement values at failure are larger, with reference to Table I.

The dramatic change in results which arise upon mesh refinement in the plastic hinge zone indicate the sensitivity of response to the location of the Gauss point in the critical section.

6.1.3. Pier model with foundation structure — no soil effects (MS3). Values of sectional and member response parameters μ_θ and μ_ϕ remain constant with their counterparts calculated in the control model. This, for reasons discussed in the previous section, should be expected. Class 3 response parameters, based on global response, once again showed a degree of variability with marginally lower values of μ_θ and μ_ϕ, as given in Table II. A reduced value of peak lateral force P_{peak} was recorded. This does not represent a drop in the capacity of the pier, but in fact indicates the greater involvement of P–Δ moments. This can be verified by checking the moment versus displacement curves for the control and model assumption. Both reach the same peak moment corresponding to the onset of strain hardening in the steel, but at different levels of displacements, as shown in Figure 10.

Displacement ductility suffers a 30 per cent reduction. This variation arises not from a change in performance of the actual pier but from the definition of μ_Δ. Due to a lower lateral stiffness of the overall structural system, considerable displacement and rotation of the piles and pile cap takes place before the lateral force required to cause yield is achieved. More than one-third of the displacement up to the point of yield occurs as elastic translation of the pile cap, with a further 15 per cent of tip displacement originating from rotation of the pile cap. Upon yield the stiffness of the pier progressively softens and its plastic deformations begin to form the significant component of the overall displacement. As a consequence of yield displacement being dominated by translation of the piles and rotation of the pile cap, reduced values of μ_Δ occur in all classes. Furthermore a comparison of energy absorbed in the plastic hinge shows consistency with the control model, as shown in Table IV.

6.1.4. Pier model with foundation structure and soil (MS4). For the same reason of reduced lateral stiffness each of the models with varying soil stiffness exhibits values of μ_Δ lower than the control model. The inclusion

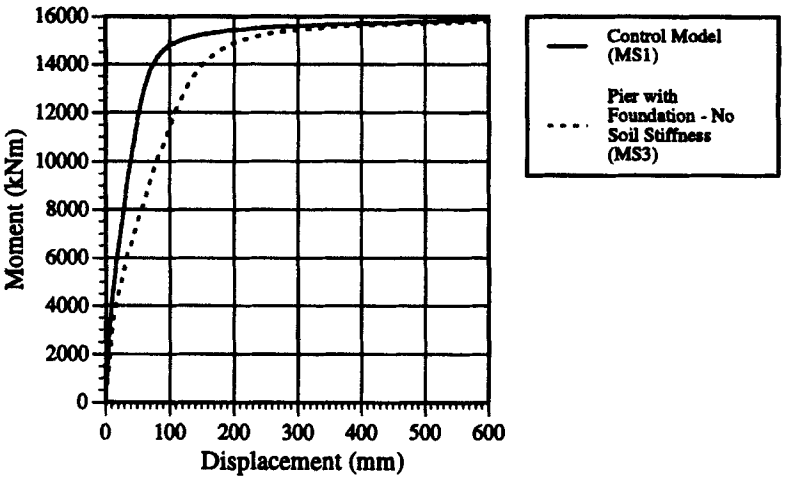

Figure 10. Moment deflection curve for control model and pier incorporating foundation structure without soil stiffness

of soil, on the other hand, increases lateral stiffness when compared to the previous system. This has the effect of reducing elastic displacements at foundation level which occur up to yield, thereby marginally increasing the values of μ_Δ with increasing stiffness. No appreciable change occurs in the values obtained for plastic hinge length.

Comparison of the family of load-deflection of curves for varying soil stiffness shows little variation of response in real terms. Over the full range of what may be considered possible sub-soil conditions only a 15 per cent variation of μ_Δ is observed. This value represents a minor degree of change when compared to the range of difference in soil stiffness used.

6.2. Deck stiffness

Response of systems which include deck stiffness changes from that of a cantilever to a more rigid shear frame behaviour, thus significantly altering the overall structural response. This is due to the pier deforming in double curvature, which allows for two possible plastic hinges to develop, changing the energy absorption characteristics. It was therefore deemed that an additional control model (MS5), a cantilever pier incorporating deck stiffness, would be necessary for purposes of comparison.

6.2.1. Cantilever model incorporating deck stiffness (MS5). The first interesting feature of the results obtained is the reversal of Classes 1 and 2 in terms of bounding values. In the previous analyses failure for Class 1 was set to a predetermined value of rotational ductility $\mu_\theta = 8{\cdot}0$. This value was chosen on the basis of previous work carried out by Elnashai and Beith[11] on pier ductilites and formed the lower bound values of response parameters. With the change in the pattern of structural response, this value of μ_θ capacity represents a value higher than the μ_θ demand imposed by defining failure in terms of an ultimate strain.

In general, curvature ductility calculated for this control model, and subsequently for the other models incorporating deck stiffness, display a 15 per cent reduction in Class 1 when compared to their counterparts behaving as cantilevers. The explanation for this lies with the critical plastic hinge. While responding in double curvature the moments generated tend to develop two plastic hinges, one at the base and the other just below the taper section. Two levels of confinement exist within the pier column: D12 @ 70 mm centres for the bottom 20 per cent of the column; and D12 @ 140 mm centres for the remainder of the height; hence the top hinge has lower confinement. As the foundations possess a degree of flexibility, more severe curvatures are imposed at the constrained upper hinge location. Lower confinement gives rise to less stress for a given strain and consequently a greater proportion of the cross section in compression. Yield is defined

in terms of steel strain, thus larger curvatures ensue at yield, while the ultimate limit state defined in terms of concrete strain will produce lower ultimate curvatures, refer to Table I. The outcome reduces the curvature ductility from $\mu_\phi = 9{\cdot}9$ to $\mu_\phi = 7{\cdot}8$ (Table II).

Finally the level of displacement ductility achieved increased by 20 per cent. Inspection of the normalized plastic hinge length however indicates an increase from $\tau = 2{\cdot}6$–$2{\cdot}9\ L$. Rotation of the plastic hinge is the integration of the curvatures over its length. Smaller curvatures result at failure, but this is offset by increased length of the plastic hinge leading to greater displacement ductility.

6.2.2. Pier incorporating foundation and deck influence (MS6). The values calculated for μ_θ and μ_ϕ remain consistent for each of the models possessing deck stiffness. However, a significantly larger drop occurs in displacement ductility than witnessed for the case of the pure cantilever when modified to include foundation effects. Again this is attributed to the definition of displacement ductility. Large values of displacement occur in order to develop the high degree of lateral load needed to produce yield. In this case the stiffness of the systems will approach that of a shear frame, whereas the cantilever has only 25 per cent of the shear frame stiffness. Thus even larger displacements develop in the soil before yield is achieved. Beyond yield, the pier stiffness drops and displacements become dominanted by the plastic response of the pier. Although the control model displayed a relatively high level of displacement ductility due to increased plastic hinge length, this is offset by response up to yield in the models including foundations.

Several interesting observations emanate from the deck stiffness variation models. The family of load-deflection curves obtained for variation in deck stiffness, as shown in Figure 9 display only minor changes for such a large difference in torsional stiffness. Also, the change of response pattern, from cantilever to shear frame, has important implications on location of critical sections where careful detailing is called for.

6.3. Summary and results

Two distinct categories exist in the results obtained. Within each category of model, with and without deck stiffness, three values are quoted for each response parameter, based on different criteria for the ultimate limit state. For those models displaying cantilever response Class 1 represents the lower bound, Class 2 the intermediate and Class 3 the upper bound. Models behaving as shear frames, however, have Class 2 as their lower bound, while Class 1 represents intermediate values.

Mesh refinement gave a structural response in nature very similar to the control case, but inelasticity was predicted at an earlier stage of loading, displacement ductility suffered a 25 per cent reduction in consequence. The stiffer fixed base control models in both categories tend to display levels of μ_Δ higher than their counterparts with soil–structure interaction. This results from the proportionally larger yield displacements due to flexibility of the ground conditions. Values obtained for μ_θ and μ_ϕ represent member and sectional parameters and in the absence of change in axial load they remain constant independent of modelling assumptions within each category. However, variation of these values did occur between categories and is attributed to the relocation of critical zones of inelasticity. Models possessing deck stiffness deform in double curvature and consequently develop two plastic hinges. The hinge which forms beneath the taper section has less confinement steel and consequently dictates failure, with lower values of μ_θ and μ_ϕ ensuing.

7. EFFECT OF GROUND MOTION CHARACTERISTICS

Seismic analysis results are affected by both the characteristics of the structural model and the earthquake acceleration time histories used. This section concentrates on the evaluation of the effect of the characteristics of natural earthquake records on seismic demand assessment. Furthermore, the effect of scaling of earthquake records, required for seismic demand assessment and the evaluation of the yield and collapse earthquakes, is investigated.

7.1. Structural model

For the dynamic analyses performed in the current section the most representative structural model was selected. To this end the model incorporating soil interaction but neglecting deck stiffness was chosen. Deck stiffness was omitted on the grounds that the pier design was not intended to mobilize any significant level of torsional moment. Evidence for this was discussed in Section 6.2.2 and confirmed by the analysis conducted by Monti and Nuti,[2] which showed that uplift at the deck–pier interface causes the pier to behave as a cantilever.

Linearly distributed mass was employed for all structural elements; piles, pile cap and the pier including a concentrated mass applied at the cantilever tip to account for the significant deck inertia. The basic Newmark two-parameter algorithm was utilized for the integration of the equations of motion. This was considered preferable to the ADAPTIC facility of algorithmicly-damped procedure which tends to reduce the force amplitude. For the model incorporating the pier and foundations a time step of $t_{step} \approx 0{\cdot}125$ s would have been sufficient, since the fundamental period of the structure is 1·25 s. However, the earthquake records used in the subsequent analyses were digitized at time intervals of 0·01 s. An integration time step of 0·02 s was chosen to preserve the earthquake signal, and to obtain an accurate solution. [It is noteworthy that the program used, ADAPTIC, applied automatic re-adjustment of time-step according to the convergence characteristics of the analysis].

7.2. Selection of earthquake ground motion input

Where the response of a structural form to general earthquake loading is being investigated it is vital to consider a wide range of earthquake records of varying characteristics, such as predominant period, frequency content and duration.

Zhu *et al.*[14] define three categories of earthquake ground motion: (a) normal ground motions exhibiting significant energy over a broad range of frequencies , (b) ground motion accelerograms possessing many large-amplitude, high-frequency oscillations, and finally (c) those records in which the significant energy is contained in a few long-duration acceleration pulses. These characteristics can be ascribed to variations in local soil conditions, epicentral distance and the magnitude and duration of event.

7.2.1. Concept of an a/v ratio. In the above study, it was proposed to use a 'peak ground acceleration to peak ground velocity' ratio as a simple but representative means of identifying characteristics of earthquake accelerograms. It is known that peak accelerations are associated with high frequencies while peak ground velocities are linked to moderate to low frequency oscillations. Thus, ground motions of the above type (b) will tend to display high a/v ratios, whilst for long-duration acceleration pulses of type (c) a low a/v ratio will prevail. Accelerograms recorded near the source of an earthquake will possess high a/v ratios, while with increasing distance the ratio will reduce. Furthermore, structures founded on rock and firm soil conditions will experience shorter-duration high-frequency excitation than those erected on softer material.

In essence a suite of accelerograms possessing a range of a/v ratios will not only reflect the range of possible soil types, with the implications on response amplification, but will also include significant seismological features likely to influence structural response.

7.2.2. Accelerograms chosen for dynamic analyses. Based on the discussion presented in the previous section earthquake records were chosen on the principle of accelerogram a/v ratios to achieve an ensemble which would envelope typical elastic response spectra. Three categories of a/v ratio were considered with the ranges as specified in the National Building Code of Canada:[15]

$$\text{low} \qquad a/v < 0{\cdot}8 \text{ g/ms}^{-1} \tag{8a}$$

$$\text{normal} \qquad 0{\cdot}8 \text{ g/ms}^{-1} \leqslant a/v \leqslant 1{\cdot}2 \text{ g/ms}^{-1} \tag{8b}$$

$$\text{high} \qquad 1{\cdot}2 \text{ g/ms}^{-1} < a/v \tag{8c}$$

Table V. Ground motion records employed in dynamic analysis. Ground motion records

Record label	Earthquake event	Recording station	Component direction
Friuli	Friuli (6 May 1976)	Tolmezzo, Italy	EW
Gazli	Gazli (17 May 1976)	Karakyr Point Uzbekistan	EW
Loma Prieta EW	Loma Prieta (17 October 1979)	Emeryville California USA	S80W
El Centro	Imperial Valley (18 May 1940)	El Centro California USA	S00E
Spitak	Spitak (17 December 1988)	Gukasyan Armenia	Translational
Loma Prieta NS	Loma Prieta (17 October 1979)	Emeryville California USA	N10W

A suite consisting of six earthquake records was used, with two records selected from each category of a/v ratio. The location and dates of the events are given in Table V along with the location and direction of the recording. This set of records was used successfully by Broderick[16] for the evaluation of behaviour factors for composite frames.

The selection consists of three Californian records, including the commonly used North–South component of the Imperial Valley earthquake recorded at El Centro in 1940, and three Eurasian records. Both the records from Emeryville during the Loma Prieta earthquake of 1989 are significantly different from the majority of records from this event as they were recorded on a site of very soft soil. Of the Eurasian events, the Gazli earthquake possesses the largest local magnitude and peak ground accelerations of the set. The Spitak accelerogram was recorded during the destructive Armenian earthquake of 1988, and finally the Friuli record is included on account of its very high a/v ratio and unusual acceleration time-history, exhibiting a single high amplitude pulse.

Further details of the properties of the recording site and peak ground motions for all six records are given in Tables VI and VII.

7.3. Variability of response due to earthquake characteristics

7.3.1. Structural behaviour factors. For a particular response period the behaviour factor q for a structure, as defined in Eurocode 8,[9] is the ratio of the ordinates of the elastic acceleration spectrum used to define the seismic hazard at a site to those of the inelastic spectrum employed in the derivation of the seismic design forces:

$$q = (S_a)_d^{el}/(S_a)_d^{in} \tag{9}$$

Table VI. Site properties of recording station and local magnitude. Recording station and magnitude of event

Record label	Epicentral distance (km)	Soil type	Magnitude M_L
Friuli	52	Rock	6·4
Gazli	14	Intermediate stiffness	7·3
Loma Prieta EW	97	Soft	7·1
El Centro	8	Stiff	6·6
Spitak	27	Intermediate stiffness	6·8
Loma Prieta NS	97	Soft	7·1

Table VII. Ground motion characteristics of accelerograms. Ground motion record properties

Record label	Peak ground acceleration (g)	Peak ground velocity (m/s)	a/v ratio (g/ms^{-1})	Period of max amplificaion (s)
Friuli	0·159	0·080	1·99	0·95
Gazli	0·724	0·606	1·20	0·13
L. Prieta EW	0·213	0·216	0·99	0·65
El Centro	0·344	0·365	0·94	0·26
Spitak	0·182	0·237	0·77	0·36
L. Prieta NS	0·250	0·438	0·58	1·20

This assumes constant amplification throughout the period range. In the above, $(S_a)_d$ denotes the design spectral acceleration and the superscripts el and in refer to the elastic and inelastic values, respectively. In Eurocode 8,[9] maximum allowable q-factors are specified for a range of structural forms and construction materials, whilst the same role is played by the parameter R (or R_w for working stress codes) in U.S. practice. These values are intended to reflect the ability of a structural type to undergo stable oscillations in the inelastic range. Furthermore, they are also intended to represent the lower bounds on actual ductility supply of individual structures. Thus it should be expected that $q_{code} \leqslant q'$, where q' represents the ultimate value not from design spectra but actual response spectra obtained from ground motion intensities which produce yield and collapse, i.e.

$$q = (S_a)_c^{el}/(S_a)_y^{el} \tag{10}$$

where subscripts 'c' and 'y' refer to collapse and yield, respectively.

Using the rationale that a perfectly designed structure will yield under the design forces corresponding to $(S_a)_{in}^{d}$, equation (10) may be re-written as

$$q' = (S_a)_c^{el}/(S_a)_d^{in} \tag{11}$$

a definition utilized by Kappos.[17] While accounting for variability in the collapse earthquake such a definition does not account for variability in ground acceleration at yield, instead adopting the design yield value. Referring back to equation (10), actual structural behaviour factor is defined as

$$q' = \frac{a_{g\ (collapse)}}{a_{g\ (yield)}} \tag{12}$$

assuming a constant dynamic magnification factor between collapse and yield spectra. This quantity accounts for variability of both the yield and collapse values. Subsequent behaviour factor values in this study are based on the definition of equation (12). It is noteworthy that alternative definitions exist, the discussion of which is beyond the scope of this work.

The approach used to calculate q factors was outlined in equation (12) and involves determining the respective values of ground motion which cause yield and collapse. Due to prohibitive times involved for computational analysis, only one class of ultimate definition was employed. The failure strain of concrete was selected for this purpose, since it represents a reasonable criterion for bridge piers, as opposed to interstorey drift often used for building frames.

Determining the values of yield and collapse earthquake can only be approached in an iterative manner, by successively scaling the earthquake record. Here, the direction acceleration scaling procedure was utilized, a decision further discussed in Section 7.3.2.1.

The values of behaviour factor evaluated for the six earthquakes, given in Table VIII show the extent to which ground motion input may cause variation due to predominant frequency, frequency content, duration and number of cycles corresponding to the particular frequencies of structural significance. The results given

Table VIII. Individual behaviour factors for each earthquake record. Behaviour factors

Record label	Yield PGA $a_{g\ (yield)}$	Ultimate PGA $a_{g\ (collapse)}$	Behaviour factor $\frac{a_{g\ (collapse)}}{a_{g\ (yield)}}$	Ratio to mean $\frac{q_i}{q_{mean}}$
Friuli	2·500	10·00	4·0	0·909
Gazli	0·305	1·010	3·3	0·75
Loma Prieta EW	0·160	0·570	3·6	0·819
El Centro	0·130	0·930	7·2	1·636
Spitak	0·130	0·665	5·1	1·159
Loma Prieta NS	0·100	0·320	3·2	0·727
Mean	—	—	4·4	—

in Table VIII, highlight the danger of using natural earthquakes in seismic assessment studies when the suite of records is not carefully selected. For instance, if Friuli., El Centro and the Spitak records were chosen, a mean q factor would have been 5·4. On the other hand, the three remaining records, if used on their own, would have indicated a mean behaviour factor of 3·3, more than 35 per cent lower than the former value. Moreover, the results show that El Centro, which is by far the most widely used earthquake record, is by no means of conservative loading scenario. Furthermore, the results for Friuli indicate the danger of applying equation (11) for behaviour factor calculation, where the yield acceleration is taken as the design acceleration. This particular record has a very narrow band of frequencies associated with high amplifications, hence all analyses using this record give rather spurious results. This was also reported by Broderick.[16]

7.3.2. Variability due to earthquake record scaling procedure. To investigate the effect of ground motion as an input parameter on demand imposed it is imperative that comparison is made with records possessing the same level of intensity. This necessity stems from the fact that all important features of seismic response, such as strength and ductility are highly dependent on ground motion intensity. Having ensured this, other features such as frequency content and duration of loading can then be examined.

Earthquake records display wide variations in intensity, thus a procedure must be employed to scale records to a common level. The effects on structural response of various scaling techniques are discussed in the following section.

7.3.2.1. Effect of ground motion scaling on seismic response

For the purpose of calculating behaviour factors, direct acceleration scaling has the advantage of simplicity in application and is consistent with methods adopted in design codes to define seismic loads. However, it has long been recognized (for example by Blume *et al.*[18]) that depending on structural period, the response may be sensitive to ground acceleration, velocity or displacement. Three ranges of structural period have been defined, corresponding to sensitivity to ground acceleration, velocity and displacement; $T < 0{\cdot}5$ s, $0{\cdot}5 \leqslant T \leqslant 3{\cdot}0$ s and $T > 3{\cdot}0$ s, respectively. Short period structures will consequently be sensitive to peak ground acceleration, while structures of moderate to long period will be sensitive to peak ground velocity. Spectral dispersion can thus be reduced for short period structures by scaling to acceleration, with similar reductions for longer periods by scaling to velocity. Such concepts have been recently re-confirmed by both Tso *et al.*[19] and Chandler.[20]

It would seem appropriate therefore to scale earthquake records in a manner which reflects the significant response periods of the structure under consideration. In the case of the pier in this study, scaling to peak ground velocity would thus be implied, in recognition of the moderately long natural period. Such a scaling procedure, however, lacks consistency with most current design code methodology and would not satisfy the equivalence between records and the design spectra. To overcome this difficulty it is possible to use acceleration scaling alongside the concept of spectral intensity proposed by Housner.[21] The latter is defined as the area under the pseudo-velocity spectrum curve between the periods of 0·1 and 2·5 s,

expressed as

$$SI(\beta) = \int_{0.1}^{2.5} S_v(T, \beta)\, dT \tag{13}$$

where β represents the fraction of critical damping, S_v the pseudo-spectral velocity and T the response period. The pseudo-spectral velocity is obtained from the integration with respect to period of the acceleration response spectrum through the following equation:

$$S_v(T_i, \beta) = \int_{0.0}^{T_i} \frac{TS_a(T, \beta)}{2\pi} dT \tag{14}$$

where S_a is the spectral acceleration.

The effect of scaling to equal spectrum intensities ensures that the earthquake records possess equal energy contents between the periods 0·1 and 2·5 s. Nau and Hall[22] demonstrated that such a procedure significantly reduces spectral dispersion for the period range under consideration. It is, however, important to state that other intensity definitions, such as the Arias intensity, may be used for scaling purposes.

7.3.2.2. Scaling of selected ground motions

In order to compare seismic demand imposed by each ground motion record, two scaling procedures were employed. The first was the simple approach adopted in normal design code practice, where peak acceleration is linearly scaled to the target value, 0·25 g for this study. The second procedure applied was scaling of each record to contain the same level of spectral intensity as the design spectrum with peak ground acceleration 0·25 g. This was achieved by firstly assessing the spectral intensity contained in each record, after linear scaling of peak ground acceleration to the design peak value of 0·25 g. Each accelerogram was then re-scaled, by its ratio of spectral intensity to the design code intensity, as indicated in Table IX.

7.3.2.3. Structural response

The results of the analysis under the two earthquake scaling procedures are presented in Tables X and XI. The displacement response time histories are given in Figures 11–16, where differences in peaks, their time of occurrence and response periods are clearly indicated; the latter is a consequence of differences in instantaneous inelastic stiffness. Use was made of the static results to construct relationships between concrete compressive strain and the ductility demand, hence the results of the analysis were used directly to assess the latter quantity.

The results further demonstrate the variability of structural response, both in terms of physical response and ductility demand. It would appear that due to its unusual single pulse nature, results obtained for the Friuli record exist rather as an anomaly, and were subsequently discounted from the results set for further

Table IX. Scaling of accelerograms to design peak ground acceleration and EC8 design spectrum spectral intensity. Scaling of ground motion accelerations

Record label	Peak ground acceleration (pga) $a_{g\ max}$	pga $\frac{a_{g\ design}}{a_{g\ max}}$	$a_{g\ (pga\ corr)}$ (g)	$SI_{(pga\ corr)}$ (m)	$\frac{SI_{EC\ 8}}{SI_{(pga\ corr)}}$	$a_{g\ (SI\ corr)}$ (g)
Friuli	0·159	1·56	0·250	143·7	1·20	0·301
Gazli	0·724	0·35	0·250	71·3	2·42	0·608
L. Prieta EW	0·213	1·17	0·250	116·3	1·48	0·371
El Centro	0·344	0·73	0·250	100·5	1·72	0·430
Spitak	0·182	1·30	0·250	95·6	1·80	0·500
L. Prieta NS	0·250	1·00	0·250	192·3	0·90	0·225

Table X. Structural response for PGA and SI scaling procedures.
Structural response

Record label	$\delta_{(max,\ pga)}$ (mm)	$\varepsilon_{(conc,\ pga)}$ $\times 10^{-3}$	$\delta_{(max,\ SI)}$ (mm)	$\varepsilon_{(conc,\ SI)}$ $(\times 10^{-3})$
Friuli	15	0·650	18	0·750
Gazli	50	1·200	115	2·750
L. Prieta EW	180	5·000	250	9·250
El Centro	130	3·000	160	4·750
Spitak	150	3·100	210	6·750
L. Prieta NS	210	7·500	210	7·000
Mean, μ	144	3·96	189	6·10
Std. dev., σ	52·3	2·14	46·7	2·20
COV $= \sigma/\mu$	**0·36**	**0·54**	**0·25**	**0·36**

Table XI. Response parameters for PGA and SI scaling procedures. Response parameters

Record label	μ_Δ (demand pga)	μ_ϕ (demand pga)	μ_Δ (demand SI)	μ_ϕ (demand SI)
Friuli	0·27	0·40	0·28	0·50
Gazli	0·75	0·80	1·55	2·00
L. Prieta EW	2·20	4·20	3·20	8·00
El Centro	1·60	2·40	2·20	3·80
Spitak	1·60	2·50	2·60	5·50
L. Prieta NS	2·75	6·50	2·70	6·00
Mean, μ	1·78	3·28	2·45	5·06
Std. dev., σ	0·67	1·94	0·55	2·03
COV $= \sigma/\mu$	**0·38**	**0·59**	**0·22**	**0·40**

Note: Values of ductility $< 1{\cdot}0$ indicate elastic response.

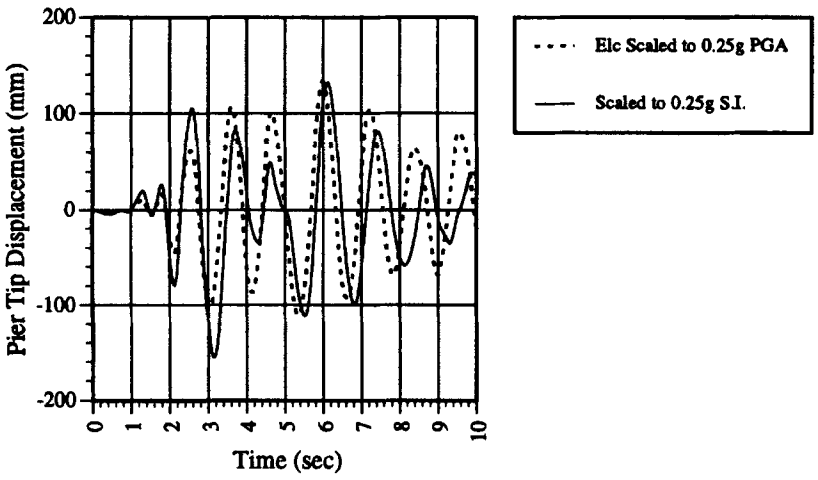

Figure 11. El Centro earthquake time-displacement response, SI and PGA scaling

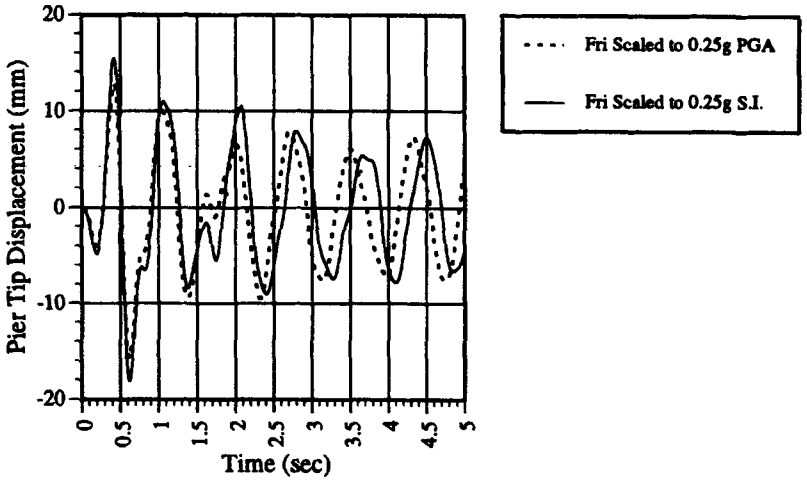

Figure 12. Friuli earthquake time-displacement response, SI and PGA scaling

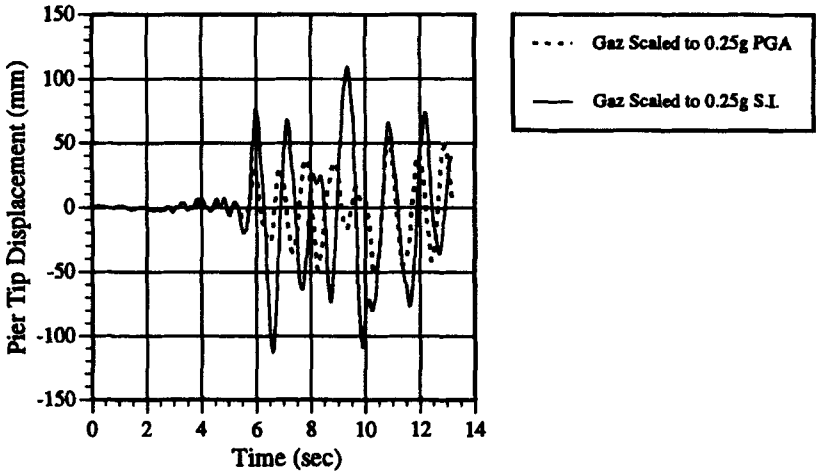

Figure 13. Gazli earthquake time-displacement response, SI and PGA scaling

evaluation. More interestingly some important features come to light from the data presented in Tables X and XI. Although not strictly applicable for such a limited data set, values of the coefficient of variation were calculated for structural response and response parameters. The outcome suggests less dispersion between results for scaling to spectral intensity, rather than peak ground acceleration.

It is evident that direct acceleration scaling takes no account of levels of spectral response at frequencies other than that associated with the peak acceleration pulse. Consequently two records which possess equal peak ground acceleration will be scaled with the same factor irrespective of their frequency content. In contrast, scaling to spectral intensity ensures that all records possess the same intensity across the response spectrum band for periods from 0·1–2·5 s, and for structures of moderate to long period, constitutes a more appropriate approach.

The results presented in Table XI indicate that the coefficient of variation of the ductility demand, though the sample is by no means statistically viable, drops by 30–40 per cent when spectral intensity scaling is used.

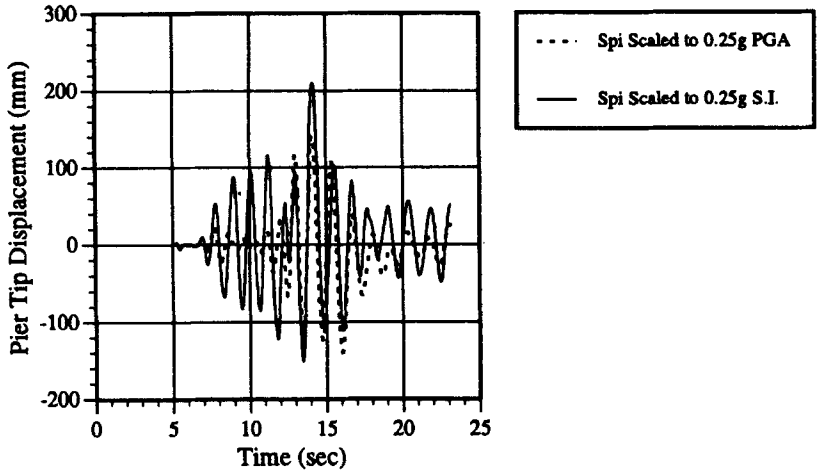

Figure 14. Spitak earthquake time-displacement response, SI and PGA scaling

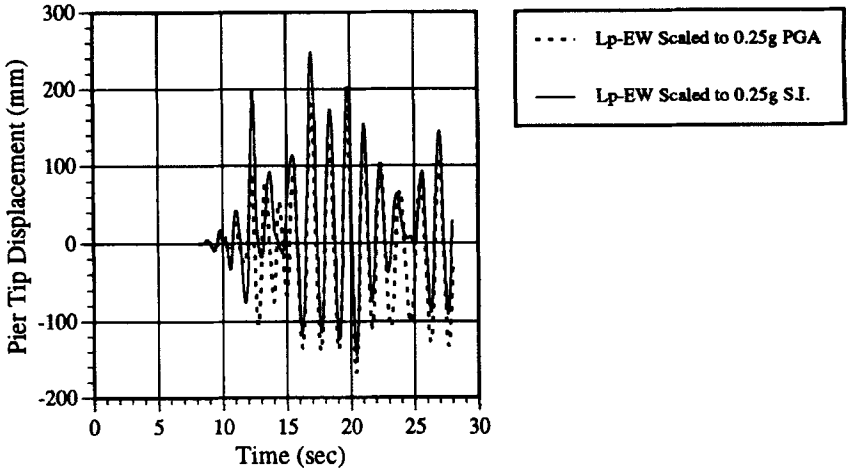

Figure 15. Loma Prieta EW earthquake time-displacement response, SI and PGA scaling

Furthermore, if the behaviour factor is defined in terms of the equivalent design code spectrum values for a given record,

$$q^* = a_{g\ (\text{collapse})}^{c} / a_{g\ (\text{yield})}^{c} \tag{15}$$

where the superscript c denotes the equivalent design code spectrum value of acceleration, for a given natural earthquake record scaled using spectral intensity, it is evident that employing spectral intensity scaling would produce behaviour factors in significant contrast to those presented in Section 7.3.1, since yield and collapse ground accelerations will be different from those given in Table VIII.

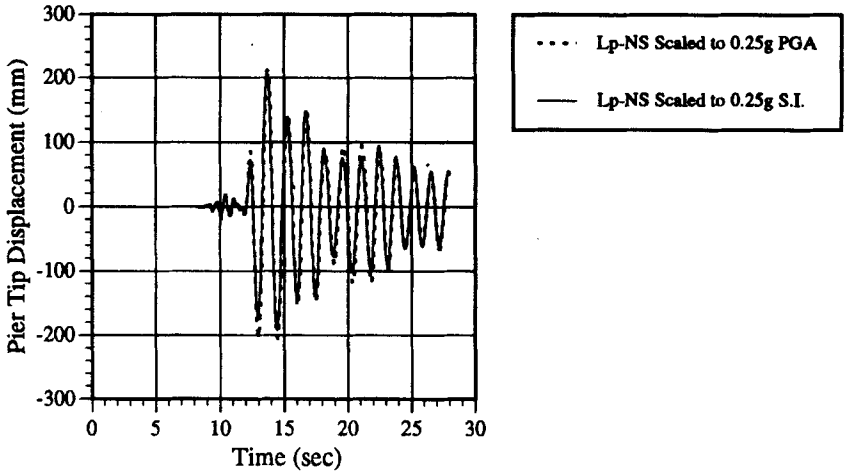

Figure 16. Loma Prieta NS earthquake time-displacement response, SI and PGA scaling

8. CONCLUSIONS AND RECOMMENDATIONS

This study is aimed at providing guidance regarding the inelastic analysis of reinforced concrete bridges under earthquake loading. Consequently, model assumptions and input motion variability have been investigated.

Mesh refinement in static analysis had little effect on the overall load–displacement response. However, due to relocation of the critical section, local ductility differed by more than 20 per cent. The inclusion of soil–structure interaction in the static analysis resulted in reduction of 15–30 per cent in displacement ductility, due to large variations in the yield limit state attainment. Moreover reductions of 25–45 per cent in displacement ductility ensued when the deck torsional stiffness was introduced. However, the effect of the variations in the soil lateral stiffness and the deck torsional stiffness are less significant, in comparison with the effect of including the modelling feature. The plastic hinge length only changed when deck stiffness was introduced. This is due to the existence of two zones of inelasticity, as opposed to one for the free cantilever. Furthermore, a 20 per cent increase in displacement ductility was observed.

The investigation into the effect of ground motion characteristics has indicated very large differences in the seismic behaviour factor q (R or R_w in U.S. practice). A carefully selected suite of earthquake records, exhibiting a range of low, medium and high peak ground-acceleration-to-velocity ratios, produced widely varying response parameters. Variations in q between 3·2 and 7·2 were recorded, a difference of 225 per cent. It is therefore concluded that seismic design codes recommending the use of a minimum of three natural earthquakes may be inadequate. No correspondence was observed between a/v ratio and behaviour factor.

The most important parameter in seismic demand evaluation using inelastic dynamic analysis is the method of earthquake scaling. Analysis of the bridge pier under two sets of records, the first scaled to a common peak ground acceleration, whilst the second scaled to a common velocity spectral intensity produced significantly different results. The latter suite, on average, imposed ductility demands 54 per cent higher than those imposed by the former, with some cases in excess of 100 per cent. Moreover, the dispersion of response parameters amongst the former records was reduced by more than 30 per cent when spectral intensity scaling was used.

Based on the analysis undertaken above, and constrained by its limitations, the following recommendations are offered to improve the quality of inelastic dynamic analysis, and to render analyses undertaken by different research groups more comparable than is currently observed:

- Mesh refinement in the plastic hinge should be adopted. Thus members in the expected zone of plasticity should be limited to $L/10$–$L/8$, where L is the length of the pier column.

- Soil–structure interaction plays a significant role in the response of the system, and thus should be included. However, only minor variations in response take place across the limits of soil stiffness.
- Displacement ductility is significantly affected by the inclusion of piles. Therefore, it should be used in seismic assessment only alongside local ductility quantities such as curvature ductility and plastic hinge length.
- Deck stiffness, if intended to be mobilized, leads to appreciable differences in response parameters, but actual sensitivity to variation in deck stiffness is minimal. Consequently only an overall idea of the likely deck dimensions is sufficient to arrive at a stiffness suitable for response parameter calculations.
- In seismic assessment of bridges, a suite of earthquake records spanning the range of peak ground-acceleration-to-velocity ratios should be employed. The minimum number of records within each of the a/v categories high, medium and low should be two, hence a suite of six earthquake records is required, as a minimum.
- When calculating seismic demand estimates for bridges, it is essential to use a scaling procedure which has an influence on the input seismic energy. The velocity spectral intensity, with $t_1 = 0{\cdot}1$ and $t_2 = 2{\cdot}5$, is a feasible technique that leads to results which are significantly more stable than direct acceleration scaling. Narrowing the period range for spectral intensity scaling may be advantageous, but this has not been studied herein.

Further work concerning the applicability of the above recommendations to more complicated models of bridge and soil systems under biaxial and asynchronous ground motion is needed. Various research groups are currently co-operating on such topics.

ACKNOWLEDGEMENTS

Partial financial support has been provided by the University of Southern California, through the research programme funded by the Carpenters/Contractors Co-operation Committee Inc. and the Commission of European Communities (Human Capital and Mobility; Prenormative Research in Support of EC8). The authors are also grateful for the help of Dr. B. A. Izzuddin in using the program ADAPTIC.

APPENDIX: NOTATION

a	acceleration
$a_{g\ (yield)}$	earthquake record peak acceleration at yield
$a^c_{g\ (yield)}$	design code spectrum peak acceleration at yield
$a_{g\ (collapse)}$	earthquake record peak acceleration at collapse
$a^c_{g\ (collapse)}$	design code spectrum peak acceleration at collapse
d_{cc}	diameter of the confined concrete core
f_{co}	compressive strength of unconfined concrete
f_l	lateral confining pressure
f_{sy}	yield strength of confining stirrups
f_{cu}	cylinder compressive strength
f_t	concrete tensile strength
f_y	characteristic steel yield
f_u	ultimate strength of steel
k_θ	deck torsional stiffness
K_σ	confinement factor
q_{code}	code behaviour factor
q'	actual behaviour factor
q^*	actual behaviour factor calculated using equivalent design code spectrum accelerations, for a given natural earthquake record, based on spectral intensity scaling

S_{sp}	spacing of the confining stirrups
$(S_a)_d^{el}$	elastic design spectral acceleration
$(S_a)_d^{in}$	inelastic design spectral acceleration
$(S_a)_c^{el}$	elastic design spectral acceleration for collapse
$(S_a)_y^{el}$	elastic design spectral acceleration for yield
SI	spectral intensity
S_v	pseudo-spectral velocity
t_{step}	numerical integration time step
v	velocity
V_c	shear contribution from concrete
V_s	shear contribution from steel reinforcement
V_p	shear contribution from axial force
V_{tot}	pier total shear capacity

Greek letters

α_c	effective confinement coefficient
β	fraction of critical damping
ε_{sy}	steel yield strain
ε_s	steel strain
ε_{sy}	strain at yield
μ	strain hardening parameter
μ_Δ	displacement ductility
μ_θ	rotational ductility
μ_ϕ	curvature ductility
ρ_s	volumetric ratio of confining steel
τ	normalized plastic hinge length

REFERENCES

1. M. Petrangeli and P. E. Pinto, 'Seismic response analysis and assessment using nonlinear and linear models', in *Proc. 2nd int. workshop on seismic design of bridges*, Queenstown, New Zealand, 1994, pp. 146–163.
2. G. Monti and C. Nuti, 'Seismic analysis of a curved continuous bridge', in *Proc. 2nd int. workshop on seismic design of bridges*, Queenstown, New Zealand, 1994, pp. 597–616.
3. J. Kodera, Y. Maehara and J. Watanabe, 'Analysis of bridge Example A: modal analysis under two different supporting conditions', in *Proc. 2nd int. workshop on seismic design of bridges*, Queenstown, New Zealand, 1994, pp. 665–684.
4. M. J. Kowalsky and M. J. N. Priestley, 'Substitute structure analysis of modern curved bridge', in *Proc. 2nd int. workshop on seismic design of bridges*, Queenstown, New Zealand, 1994, pp. 203–221.
5. S. P. Singh and G. L. Fenves, 'Earthquake response of structure a using nonlinear dynamic analysis', in *Proc. 2nd int. workshop on seismic design of bridges*, Queenstown, New Zealand, 1994, pp. 222–239.
6. S. Dodd, A. S. Elnashai, B. A. Izzuddin and G. M. Calvi, 'A 3D nonlinear dynamic analysis of a curved bridge', in *Proc. 2nd int. workshop on seismic design of bridges*, Queenstown, New Zealand, 1994, pp. 617–640.
7. G. A. Chan and J. B. Mander, 'Seismic energy based fatigue damage analysis of bridge columns: part II — evaluation of seismic demand', *National Centre for Earthquake Engineering Research Technical Report NCEER-94-0013*, 1994.
8. P. J. Madas and A. S. Elnashai, 'A theoretical model for composite beam-columns under cyclic loading', *Imperial College, Engineering Seismology and Earthquake Engineering Report No. 89/10*, 1989.
9. EC8, Eurocode8: Earthquake Resistant Design of Structures, ENV1998, CEN, 1992.
10. J. B. Mander, M. J. N. Priestley and R. Park, 'Theoretical stress–strain model for confined concrete', *J. struct. eng. ASCE* **114**, 1804–1826 (1988).
11. A. S. Elnashai and J. G. Beith, 'Seismic design limit states and analytical ductility supply of circular bridge piers', in *Proc 2nd int. workshop on seismic design of bridges*, Queenstown, New Zealand, 1994, pp. 310–364.
12. G. Lappas and T. P. Tassios, 'Estimation of behaviour factors of RC buidlings', *Eur. earthquake eng.* **3**, 38–42 (1988).
13. R. Park (ed.), 'Comparative bridge examples', in *Proc 2nd int. workshop on seismic design of bridges*, Queenstown, New Zealand, 1994, pp. 567–578.
14. T. J. Zhu, A. C. Heidebrecht and W. K. Tso, 'Effect of peak ground acceleration to velocity ratio on ductility demand of inelastic systems', *Earthquake eng. struct. dyn.* **16**, 63–79 (1988).
15. NBCC: Associate Committee on the National Building Code, *National Building Code of Canada 1985*, National Research Council of Canada, Ottawa, Ontario, 1985.
16. B. M. Broderick, 'Seismic testing, analysis and design of composite frames', *Ph.D. Thesis*, Imperial College, University of London, 1994.

17. A. J. Kappos, 'Analytical prediction of the collapse earthquake for RC buildings: suggested methodology', *Earthquake eng. struct. dyn.* **20**, 167–176 (1991).
18. J. A. Blume, N. M. Newmark and L. H. Corning, *Design of Multistory Reinforced Concrete Buildings for Earthquake Motions*, Portland Cement Association, 1961.
19. W. K. Tso, T. J. Zhu and A. C. Heidebrect, 'Engineering implications of ground motion A/V ratio', *Soil dyn earthquake eng.* **11**, 133–144 (1992).
20. A. M. Chandler, 'Evaluation of site-dependent spectra for earthquake-resistant design of structures in Europe and North America', *Proc. ICE*, London, Part 1, **90**, 605–626 (1991).
21. G. W. Housner, 'Spectrum intensity of strong-motion earthquakes', in *Proc. symp. earthquake and blast effects on structures*, UCLA, 1952, pp. 20–36.
22. J. M. Nau and W. J. Hall, 'Scaling methods for earthquake response spectra', *J. struct. eng. ASCE* **110**, 1533–1548 (1984).